doi:10.2109/jcersj2.121.291

Electron–phonon coupling and defect scatterings in Ar^+-ion implanted graphite

Ikufumi KATAYAMA, Sho KOGA, Jun TAKEDA, Shunichi HISHITA,[*] Daisuke FUJITA[**] and Masahiro KITAJIMA

Graduate School of Engineering, Yokohama National University, Yokohama 240–8501, Japan
[*]Optical and Electronic Materials Unit, National Institute for Materials Science, Tsukuba, Ibaraki 305–0044, Japan
[**]Nano Characterization Unit, National Institute for Materials Science, Tsukuba, Ibaraki 305–0047, Japan
[***]Department of Applied Physics, National Defense Academy, Yokosuka, Kanagawa 239–8686, Japan

Journal of the Ceramic Society of Japan 121 [3] 291-294 2013 Reprint

Journal of the Ceramic Society of Japan 121 [3] 291-294 2013 Paper

Electron–phonon coupling and defect scatterings in Ar^+-ion implanted graphite

Ikufumi KATAYAMA, Sho KOGA, Jun TAKEDA,† Shunichi HISHITA,* Daisuke FUJITA and Masahiro KITAJIMA‡**

Graduate School of Engineering, Yokohama National University, Yokohama 240–8501, Japan
***Optical and Electronic Materials Unit, National Institute for Materials Science, Tsukuba, Ibaraki 305–0044, Japan**
****Nano Characterization Unit, National Institute for Materials Science, Tsukuba, Ibaraki 305–0047, Japan**
*****Department of Applied Physics, National Defense Academy, Yokosuka, Kanagawa 239–8686, Japan**

Dynamics of coherent G-mode and D-mode phonons in Ar^+-ion implanted graphite has been investigated using transient reflectivity measurement. With an increase in the Ar^+-ion dose, coherent D-mode phonon appears at which the dephasing rate of the coherent G-mode phonon begins to increase. The increase in the amplitude of the coherent D-mode phonon and those in dephasing rates of the coherent D-mode and G-mode phonons indicate effective carrier-defect scatterings in the defective graphite. The dephasing rate of the D-mode is larger than that of the G-mode, indicating an existence of an additional dephasing process for the D-mode. We attribute it to the broad spectral distribution of the D-mode phonon, which is understood as a coherent excitation of large wavevector phonons with different wavevectors through inter-Dirac-cone scattering. The frequency chirping of the D-mode and its defect density dependence are also discussed based on this scattering mechanism.

Key-words : Graphene, Graphite, Coherent phonons, Ultrafast spectroscopy

[Received October 1, 2012; Accepted December 24, 2012]

Carbon materials, especially graphene and carbon nanotubes, have been attractive candidates for the next generation electronics.[1),2)] These materials are categorized as ideal low-dimensional systems in which many interesting physics are revealed, such as a conical electronic dispersion in graphene and strong van-Hove singularities in carbon nanotubes. These interesting carrier and electronic properties are often perturbed by lattice and defects, and therefore, for electronic applications such as high-speed signal processing, it is essential to clarify the dynamical properties of carriers and its interaction with phonons and defects. In carbon materials, importance of the electron–phonon coupling has been pointed out in relation to Kohn anomaly and Landau damping of the highest optical phonon mode.[3),4)] Recent investigations of coherent phonons have provided a key to understand the dynamical aspects of the electron–phonon couplings in carbon materials.[5)]

However, coherent phonon experiments mostly probe phonons at the Γ point, and quantitative understanding of the phonon dynamics at different wavevectors has not fully been established. Fortunately, extensive studies on carbon materials using conventional Raman spectroscopy[6),7)] have revealed that the strong electronic resonance enables us to observe the Raman signal from large wavevector phonons through the doubly resonant Raman scattering process. This phonon, so-called D-mode phonons, often appears in defective carbon materials.[8),9)] Since the D-mode is considered as originated from the bulk phonons near the K point of the Brillouin zone, it directly couples with the Dirac electrons to show Kohn anomaly. Therefore, the dynamics of D-mode phonon is quite important in understanding the electron–phonon couplings and also the defect scatterings in carbon materials.

† Corresponding author: J. Takeda; E-mail: jun@ynu.ac.jp
‡ Corresponding author: M. Kitajima; E-mail: kitaji@nda.ac.jp

Although coherent D-mode phonons have already been observed in graphene and in carbon nanotubes,[10)–12)] the quantitative analysis of the dynamics is still lacking. In this paper, we investigated coherent phonon dynamics as well as responses of photoexcited carriers in Ar^+ ion implanted graphite by changing the ion implantation doses, namely the number of defects generated in graphite. The results demonstrate the strong dependence of the dynamical properties of phonons on the defect density, which enables us to obtain new insights into the origin of frequency chirping (upshift) of the coherent D-mode phonons, and the close relation between D- and G-mode dephasing processes. The results are discussed in terms of electron–phonon coupling, electron-defect scattering and the doubly resonant Raman scattering, showing importance of inter-Dirac-cone scattering for the photoexcited carriers.

The sample we used was highly oriented pyrolitic graphite (HOPG) whose surface was implanted with 30 keV Ar^+-ion beams in order to generate local defects. A Ti:sapphire laser with 7.5-fs pulse duration was used to excite and detect high-frequency coherent phonons in graphite. The output of the laser was separated into two beams; one was used as a pump beam to excite the coherent phonons and the other was used as a probe. The transient reflectance was measured with an electro-optic sampling method that could detect the anisotropic reflectivity change caused by the pump pulse. The delay between pump and probe beams were controlled by using an optical shaker with 15 ps scanning range at 20 Hz. Two photodiodes detected horizontal and vertical polarization components of the reflected probe light, and the difference signal was amplified and analyzed by a personal computer.

Figure 1(a) shows the obtained results of the transient reflectivity changes. With an increase in the Ar^+-ion implantation dose, the change in reflectivity gradually reduces and the

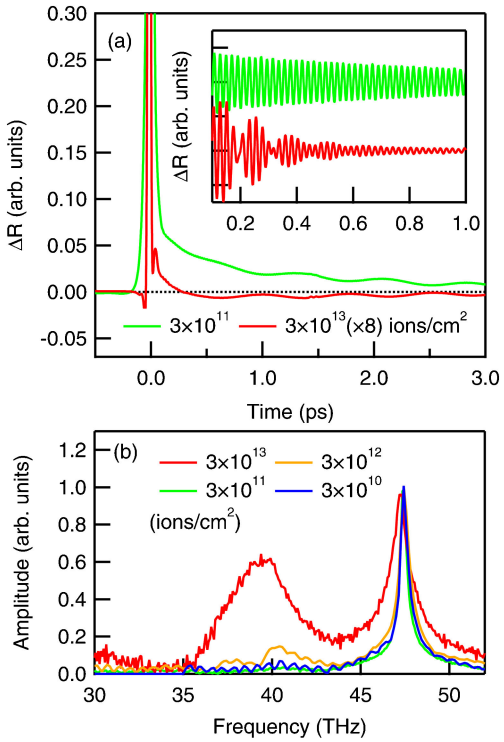

Fig. 1. (Color online) (a) Transient reflectivity change in Ar^+-ion implanted HOPG with different implantation doses. The inset shows the high-frequency coherent phonons extracted from the time profile. (b) The spectra are normalized by the G-mode intensity.

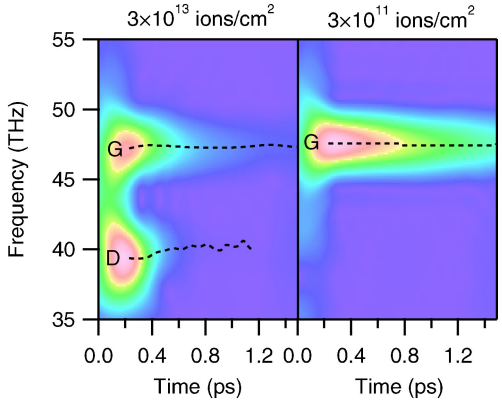

Fig. 2. (Color online) The result of the time-windowed Fourier transformation. Hanning window with the FWHM of 0.3 ps is used, and is scanned from the time origin to 1.2 ps with 0.01 ps step. Dashed lines in the figure shows the peak positions for both G- and D-modes.

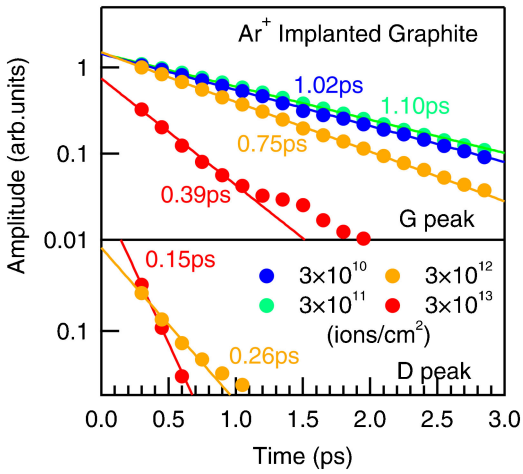

Fig. 3. (Color online) Relaxation dynamics of G- and D-modes observed in graphite samples with different Ar^+-ion implantation doses. Lines are the fitting by the single exponential decay and the numbers are the corresponding decay time for each data.

Table 1. Dephasing rates of G- and D-modes and their difference in HOPG samples with several Ar^+ ion implantation doses

Ar^+ ion dose	τ_G^{-1} (ps^{-1})	τ_D^{-1} (ps^{-1})	Δ (ps^{-1})
3×10^{10}	0.91	—	—
3×10^{11}	0.98	—	—
3×10^{12}	1.3	3.8	2.5
3×10^{13}	2.6	6.7	4.1

decay time of electronic response (carriers) becomes faster. This dependence of the decay time is similar to that observed in Ref. 13). By subtracting this electronic response and low-frequency responses, we observe coherent oscillations of high-frequency phonons in graphite as shown in the inset of Fig. 1(a). After Fourier transformation, we clearly see the C=C stretching mode of graphite (G-mode at 47.4 THz) and the D mode (40 THz) as shown in Fig. 1(b). The intensity of the D-mode increases with increasing the ion-implantation dose. The increase directly related to the creation of point defects in graphite due to Ar^+ ion implantation.[14)]

In order to investigate the dynamical aspects of the observed coherent phonons in graphite, we performed time-windowed Fourier transformation of the obtained time-profile of the high frequency coherent phonons (see the inset of Fig. 1). From the obtained time-frequency image shown in **Fig. 2**, we can deduce the relaxation dynamics of the coherent phonons, i.e. the dephasing time and the time-dependent frequency shift (chirping). In **Fig. 3**, we summarize the time evolution of the G- and D-mode amplitudes, which decreases exponentially with time. The dephasing time strongly depends on the defect density. Both mode exhibit the decrease of the dephasing time with increasing in the Ar^+-ion implantation doses, suggesting that the defect scattering plays an important role for the phonon dynamics. The obtained results of the dephasing times are summarized in **Table 1**.

Interesting point here is that D-mode phonon is observed when the dephasing time of the G-mode phonon begins to decrease. This complementary behavior can be explained by the generation mechanism of D-mode phonons, namely the doubly resonant Raman scattering process.[6),7)] In this model, D-mode phonon is excited by the defect scattering of photoexcited electrons between two resonant electronic states in the neighboring Dirac cones. Therefore, the appearance of the D-mode phonons is closely related to the existence of electron-defect scattering. On the other hand, the decrease of the G-mode dephasing time indicates the increase of phonon-defect scattering. The result, therefore, demonstrates that phonon-defect scattering and electron-defect scattering appears at nearly the same defect density. The reason for this similarity could be due to the strong electron–phonon coupling because of the Kohn anomaly in graphene.[3)]

From the time-frequency mapping of the coherent phonons, we can also evaluate the frequency chirping. The dashed lines in Fig. 2 indicate the temporal behavior of peak frequencies for the G- and D-modes. **Figure 4** summarizes the defect density dependence of these phonon chirps. As seen in Fig. 4 the

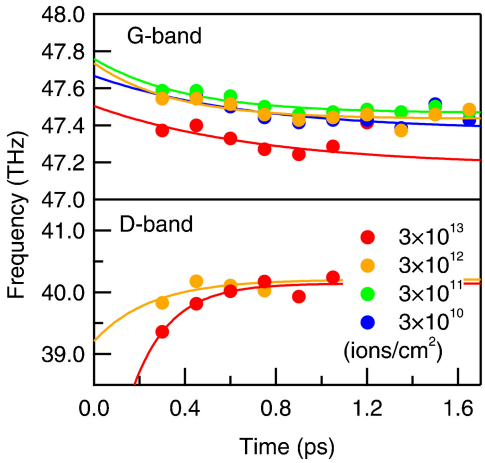

Fig. 4. (Color online) Chirping of the G-mode and D-mode coherent phonons with different ion-implantation doses. Lines are the guides for eyes.

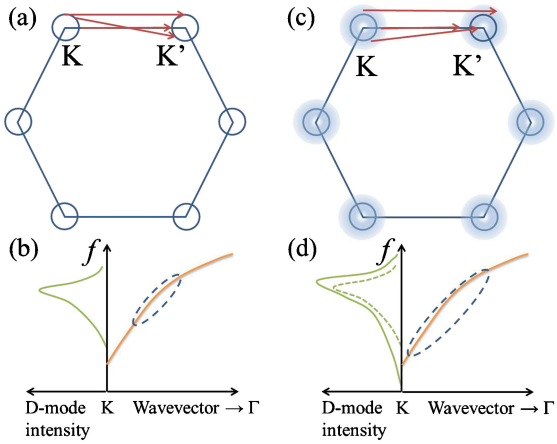

Fig. 5. (Color online) (a) Schematic of the D-mode generation mechanism via the doubly resonant Raman scattering process. Arrows indicates the possible scattering wavevectors, and rings are the excited electrons in the k-space. (b) The D-mode dispersion curve (right) and the schematic of the D-mode spectrum (left). The dashed circle indicates the wavevector region of the excited D-mode. (c) Schematic of the D-mode generation in the defective graphite. The electronic band structure blurs due to the high defect concentration. (d) The D-mode spectrum excited in defective graphite and the corresponding region in the dispersion curve (the dashed circle).

amount of the frequency shift of the G-mode phonon is almost independent of the defect density whereas that of the D-mode phonons depend on the defect density. In addition, the direction of the chirping is different between these modes. These results suggest that origin of the chirping of the D-mode might be different from that of the G-mode coherent phonons. Note that G-mode phonon chirping is considered as originated from the melting of Kohn anomaly at Γ point.[5)]

One of the important differences between G- and D-modes is that the G-mode is originated from normal first-order Raman process, while the D-mode is originated from the doubly resonant Raman scattering process. Through the doubly resonant Raman scattering process, we can excite phonons with large wavevectors ($k \neq 0$) near the K-point (D-mode),[7)] where the phonons have a linear dispersion due to the strong electron–phonon coupling (Kohn anomaly).[3)] Considering all possible scattering processes of the doubly resonant Raman scattering, excited phonon spectrum can be calculated to have an asymmetric shape with broad bandwidth as shown in Ref. 15) [see also **Figs. 5**(a) and 5(b)]. We recently propose that this asymmetric spectrum gives rise to the negative frequency chirping.[16)] The reason why this asymmetric spectrum causes frequency chirping is qualitatively understood if we consider that the observed spectrum consists of two different modes: one has high frequency with longer dephasing time, and the other has slightly lower frequency with shorter dephasing time. Because the latter mode disappears faster than the former, the peak frequency shows upshift as a function of delay time. Note that the G-mode has only a single small wavevector $k \sim 0$ due to the momentum conservation in the normal Raman process, and therefore does not have this chirping mechanism.

Within this model, the increase of the frequency chirping is attributed to the increase of the asymmetry in the D-mode phonon spectrum. With an increase in the implantation dose, the defect density becomes very high, leading to blurring the electronic band structure of the graphite (or increasing the damping of electrons). This changes the possible scattering wavevectors for excited electrons as shown by the arrows in Fig. 5(c). Since the defect scattering affects the possible wavevectors of D-mode phonons, the D-mode phonon spectrum might be wider as shown in Fig. 5(d). Because the D-mode dispersion curve has a negative curvature [see orange curves in Figs. 5(b) and 5(d)], the asymmetry of the distribution function of the D-mode is extended toward the lower wavevector as indicated by the dashed circle in Fig. 5(d). The change in the asymmetry of the D-mode phonon spectrum leads to an increase of the frequency chirping in the highly ion-implanted graphite sample.

The dephasing processes of coherent phonons in graphite are discussed as follows. Normally, the dephasing rate of phonons consists of that due to the anharmonicity and that due to the defect or impurity scatterings. However, since the D-mode spectrum consists of many phonons with different wavevectors as discussed above, an additional dephasing mechanism should be considered for the D-mode. Here, we define difference between the dephasing rates of the G- and D-modes (τ_G and τ_D, respectively) as,

$$\Delta = \frac{1}{\tau_D} - \frac{1}{\tau_G}. \quad (1)$$

Then, Δ represents the information on the additional dephasing process caused by the simultaneous excitation of many phonons allowed by the double resonance. Here, we assumed that defect and impurity scattering rate and the anharmonic phonon decay rate are the same for both G- and D-modes since the frequency of these phonons are almost the same. The estimation of Δ is also tabulated in Table 1.

The dephasing rate due to the wide spectrum of the D-mode was estimated from the theoretically calculated D-mode spectrum.[15)] The estimated dephasing time was 0.3 ps (3.3 ps^{-1}), which is in qualitative agreement with the observed Δ values in Table 1. The increase of Δ as a function of defect density may be related to the increase of the D-mode bandwidth (correspondingly the dephasing time) due to the blurring of the electronic states as discussed in Figs. 5(c) and 5(d).

In summary, we observed the coherent phonons in Ar^+-ion implanted graphite with different ion implantation doses. The D-mode dephasing rate, as well as the G-mode dephasing rate, increases with an increase in the ion-implantation dose, indicating that defect scattering is a key to understand the D-mode

phonon dynamics. The phonon chirps for both G- and D-modes are also observed with opposite signs. The different behavior of coherent G- and D-mode phonons could be originated from the different generation mechanism of the phonons, and suggests the broad wavevector distribution of the D-mode. These results demonstrate that observation of dynamical behaviors through coherent phonon experiment is important in understanding the electron–phonon couplings and defect scatterings in carbon materials.

Acknowledgments This work was partially supported by the Ministry of Education, Culture, Sports, Science and Technology through KAKENHI (Grant Nos. 20671002, 21104510, 23241034, and 23104515). IK also acknowledges the financial support received through the Special Coordination Funds for Promoting Science and Technology from the Japan Science and Technology Agency (JST).

References

1) S. Reich, C. Thomsen and J. Maqultzsch, "Carbon Nanotubes", Wiley-VCH, Weinheim (2004).
2) A. K. Geim and K. S. Novoselov, *Nat. Mater.*, 6, 183–191 (2007).
3) S. Piscanec, M. Lazzeri, F. Mauri, A. C. Ferrari and J. Robertson, *Phys. Rev. Lett.*, 93, 185503 (2004).
4) J. Yan, Y. Zhang, P. Kim and A. Pinczuk, *Phys. Rev. Lett.*, 98, 166802 (2007).
5) K. Ishioka, M. Hase, M. Kitajima, L. Wirtz, A. Rubio and H. Petek, *Phys. Rev. B*, 77, 121402 (2008).
6) R. Saito, A. Jorio, A. G. S. Filho, G. Dresselhaus, M. S. Dresselhaus and M. A. Pimenta, *Phys. Rev. Lett.*, 88, 027401 (2002).
7) C. Thomsen and S. Reich, *Phys. Rev. Lett.*, 85, 5214–5217 (2000).
8) K. Nakamura and M. Kitajima, *Phys. Rev. B*, 45, 78–82 (1992).
9) M. J. Matthews, M. A. Pimenta, G. Dresselhaus, M. S. Dresselhaus and M. Endo, *Phys. Rev. B*, 59, R6585–R6588 (1999).
10) S. Koga, I. Katayama, S. Abe, H. Fukidome, M. Suemitsu, M. Kitajima and J. Takeda, *Appl. Phys. Express*, 4, 045101 (2011).
11) I. Katayama, S. Koga, K. Shudo, J. Takeda, T. Shimada, A. Kubo, S. Hishita, D. Fujita and M. Kitajima, *Nano Lett.*, 11, 2648–2654 (2011).
12) K. Kato, K. Ishioka, M. Kitajima, J. Tang, R. Saito and H. Petek, *Nano Lett.*, 8, 3102–3108 (2008).
13) K. Ishioka, M. Hase, M. Kitajima and K. Ushida, *Appl. Phys. Lett.*, 78, 3965 (2001).
14) D. Marton, K. J. Boyd, T. Lytle and J. W. Rabalais, *Phys. Rev. B*, 48, 6757–6766 (1993).
15) K. Sato, R. Saito, Y. Oyama, J. Jiang, L. G. Cançado, M. A. Pimenta, A. Jorio, G. G. Samsonidze, G. Dresselhaus and M. S. Dresselhaus, *Chem. Phys. Lett.*, 427, 117–121 (2006).
16) I. Katayama, K. Sato, S. Koga, J. Takeda, S. Hishita, H. Fukidome, M. Suemitsu and M. Kitajima, in preparation.